Renewable Energy 221 (2024) 119824

Contents lists available at ScienceDirect

Renewable Energy

journal homepage: www.elsevier.com/locate/renene

Hydrostatic stability and hydrodynamics of a floating wind turbine platform integrated with oscillating water columns: A design study

Payam Aboutalebi [a,b,*], Aitor J. Garrido [b], Izaskun Garrido [b], Dong Trong Nguyen [a], Zhen Gao [a,c]

[a] Department of Marine Technology, Norwegian University of Science and Technology (NTNU), Trondheim, 7491, Norway
[b] Automatic Control Group–ACG, Institute of Research and Development of Processes–IIDP, Department of Automatic Control and Systems Engineering, Faculty of Engineering of Bilbao, University of the Basque Country–UPV/EHU, Po Rafael Moreno no3, Bilbao, 48013, Spain
[c] School of Naval Architecture, Ocean and Civil Engineering, Shanghai Jiao Tong University, Shanghai, 200240, China

ARTICLE INFO

Keywords:
Semisubmersible floating wind turbine
Hydrostatic stability
Hydrodynamics
Oscillating water columns

ABSTRACT

One of the challenges in the installation of Floating Wind Turbines (FWTs) is the occurrence of undesired resonant motions under environmental conditions, which adversely impact their lifespan, maintenance cost, components stress, and electrical performance. This article addresses this challenge by proposing a novel design for the substructure of semisubmersible FWTs, aimed at mitigating the undesired oscillations and improving sustainability. The design concept involves integrating Oscillation Water Columns (OWCs) within the FWT's substructure, focusing on a specific type of semisubmersible FWT called WINDMOOR. The chambers have been incorporated into the columns, allowing water to enter and compress/decompress the air inside them. The main objective of this article is to demonstrate the feasibility of integrating OWCs into a semi-submersible platform-type FWT. To accomplish this, the adjustment of ballast inside the substructure is performed, followed by evaluations of the system's intact hydrostatic stability and hydrodynamic performance. Sensitivity analysis has also been conducted to assess the impact of the chamber size on system performance. The results indicate that a chamber size of 4.5 m satisfies the criteria for intact hydrostatic stability without requiring changes to the substructure dimensions. However, increasing the chamber size negatively affects system stability. Furthermore, the hydrodynamic analysis employing Response Amplitude Operators (RAOs) illustrates the effectiveness of integrating OWCs to enhance the stability of this novel hybrid system. This integration results in increased damping effects, which contribute to the reduction of resonant motions in the system's modes, particularly heave, roll, and pitch. Throughout the article, comprehensive comparisons have been conducted between the WINDMOOR FWT and the proposed hybrid semisubmersible FWT-OWCs system. These comparisons have been performed at every step, including the redesign of the substructure, adjustment of ballast, hydrostatic stability analysis, and hydrodynamic analysis.

1. Introduction

The desire for clean and sustainable energy sources has resulted in the increased use of renewable energy technology such as Floating Wind Turbines (FWT), Wave Energy Converters (WEC), and tidal turbines. These structures have benefits such as greater wind speeds and predictable wave patterns in offshore sites, resulting in enhanced energy output [1]. In this regard, the European Commission has established targets for the offshore renewable energy sector to support the EU's energy and climate objectives, aiming for at least 60 GW of offshore wind and 1 GW of ocean energy by 2030, and 300 GW and 40 GW respectively by 2050 [2], as part of its strategy to promote sustainable long-term development, reduce greenhouse gas emissions, and increase energy security. However, implementing marine structures for renewable energy generation is not without challenges, and one of the most significant is the negative effects of oscillatory motion on FWT systems.

Oscillations in FWT systems can be caused by a variety of factors, such as wind and wave forces, rotor-induced forces, and control system operations. The wind and wave forces acting on the turbine and its support structure may cause oscillations, especially in rough sea conditions [3]. The oscillations in FWT systems occur at different frequency ranges, encompassing resonant motions at the natural frequencies of the system's modes of motion induced by wind loads and second-order wave loads. Additionally, wave frequency motions occur due to first-order wave loads, while structural vibrations can arise from wind loads. The rotation of the blades may induce vibrations in the tower and its

* =Corresponding author at: Department of Marine Technology, Norwegian University of Science and Technology (NTNU), Trondheim, 7491, Norway.
E-mail addresses: payam.aboutalebi@ntnu.no (P. Aboutalebi), aitor.garrido@ehu.eus (A.J. Garrido), izaskun.garrido@ehu.eus (I. Garrido), dong.t.nguyen@ntnu.no (D.T. Nguyen), zhen.gao@ntnu.no (Z. Gao).

https://doi.org/10.1016/j.renene.2023.119824
Received 24 August 2023; Received in revised form 18 November 2023; Accepted 14 December 2023
Available online 16 December 2023

platform [4], and errors in the feedback loop or the algorithm design of the control system can also lead to oscillations [5].

The negative impacts of oscillatory motion on FWTs include reduced energy efficiency, higher maintenance costs, and safety issues [6,7]. The constant movement of waves causes the platform to pitch, which reduces the turbine's ability to generate electricity at peak capacity [8]. These oscillations also affect the mean power output and lead to higher power variations. Additionally, the oscillatory motion can increase the motion responses and structural loads, leading to additional stress and fatigue to the structure, increased maintenance and repair expenses over time and reduced lifespan. In severe cases, the motion may even result in structural damage, leading to downtime and loss of revenue [9]. Oscillations in wind turbines can also pose safety concerns, potentially leading to mechanical failure or collapse, and also contribute to noise pollution, which can negatively impact the nearby environment.

There are several design choices and technologies that can help reduce the effects of wind gusts and waves on FWTs. A method for minimizing oscillations in FWTs is active control systems. These systems employ sensors and control algorithms that adjust the nacelle's orientation, the floating platform's position, or the pitch angle of the blades. Examples of active systems that can be utilized to reduce the oscillations induced by wind and waves include active damping control and active yaw control systems [10,11]. Another method for minimizing oscillations in FWTs is passive damping systems. To reduce oscillations by dissipating energy, these systems consist of passive components such tuned mass dampers [12], viscous dampers [13], or pendulum dampers [14]. These devices are frequently utilized to reduce the vibrations caused by waves on the floating platform. A third option for decreasing oscillations in FWTs is aerodynamic modifications. Changes to the shape of the blades or the position of winglets or vortex generators [15–17] can all be made to decrease the aerodynamic loads on the turbine and hence the oscillations. Another possibility for decreasing oscillations in floating wind turbines is structural modifications. These adjustments include alterations to the turbine's structural design, such as the use of composite materials [18] or novel platform designs [19], to increase stiffness and reduce oscillation susceptibility. Therefore, optimization processes are vital in the design of FWT substructures, offering a cost-effective approach that considers environmental load uncertainties and lifetime costs [20]. As the installations are exposed to dynamic and variable Metocean conditions, the role of optimization in ensuring safety and performance is paramount [21]. Several recent studies have demonstrated the capacity of these processes to significantly reduce long-term fatigue damage [22] and enhance reliability, contributing to the reduction of the Levelized Cost of Energy (LCOE). Given the evolving offshore environments and growing interest in renewable energy solutions, the integration of optimization techniques into the design of floating wind turbine substructures [23,24] becomes increasingly relevant and vital. Moreover, another method for decreasing oscillations in FWTs is control strategies for reducing dynamic loads. These solutions try to lower the turbine's dynamic stresses by altering the blade pitch angle, generator torque, or power output based on measured wind and wave conditions [25–27].

The structural modification can also include the integration of WECs within FWTs for both energy harvest and oscillation reduction. The use of WECs can reduce the overall motion of the floating platform, which can in turn reduce the oscillations in the wind turbine [28]. This approach provides a dual benefit of generating renewable energy while also improving the performance and longevity of the FWTs. The researchers have integrated the WECs within FWTs for the sake of energy harness improvement [29,30]; for instance, the integration of rotating flap WECs in a semi-submersible FWT [31], the use of point absorbers in a tension leg-type FWT [32], combined tension leg-type FWT and WECs [33], and hybrid semi-submersible FWT-OWCs [34]. However, the integration of WECs in FWTs have been investigated by few researchers. In [35,36], the combined OWCs and barge-type FWT were proposed under different sea states. In [7], it was showed that the attachment of WECs in spar-type FWT can reduce the platform motion. In [37], the performance of the incorporation of OWCs in a type of semi-submersible platform FWT was evaluated. Our study is motivated by the need to address two significant research gaps within the domain of offshore wind energy: A research void exists as existing models have not been applied to semisubmersible platforms for stability purposes. Our study endeavors to fill this gap by investigating the potential for enhancing platform stability. In addition, the integration of OWCs into the platform's design has been underexplored due to a lack of detailed hydrostatic and hydrodynamic evaluations. This study aims to bridge this gap by providing a comprehensive assessment of the feasibility of OWC integration.

This article investigates the feasibility of integrating two OWCs into a semi-submersible platform-type FWT. The study focuses on a novel platform design that aims to reduce resonant motions by increasing the damping effect provided by the OWCs. The FWT's column ballast was readjusted to achieve static balance, and both hydrostatic stability and hydrodynamic analyses have been conducted to ensure system stability. Lastly, a comparative study has been conducted between the original FWT and the FWT-OWCs system, providing valuable insights into the system's performance. The research study incorporates advanced tools such as GeniE [38] and HydroD [39], developed and marketed by DNV, for platform design and hydrostatic analysis, as well as the utilization of WADAM [40] for hydrodynamic analysis. These tools, renowned for their robustness and accuracy, enable comprehensive investigations into the design and performance of the platform under various hydrodynamic conditions. By integrating these software tools, the research aims to enhance the understanding of the platform's behavior.

This article is structured into several sections that systematically investigate the incorporation of OWCs in a semi-submersible FWT. Section 2 outlines the methods used to model the systems, including the design of the fixed ballast inside the columns of the semi-submersible platform, with and without OWCs, while Section 3 presents the equations of motions for FWTs. Section 4 evaluates the hydrostatic stability of both FWT designs using intact criteria. In Section 5, a comparative analysis of the hydrodynamic characteristics of both systems is conducted, using RAOs. Finally, Section 6 presents the significant conclusions of the study and outlines potential avenues for future research.

2. Designing of FWT-OWCs hybrid system

To ensure an accurate representation of the behavior of the real model, this research study undertook three different modeling approaches, including a mass model, a panel model, and a Morison model for both original model without OWCs and the hybrid semi-submersible FWT-OWCs.

The first modeling approach employed in this study focuses on mass modeling, wherein the mass distribution throughout the entire system has been incorporated. The original FWT model, referred to as the INO WINDMOOR [41], has undergone a design and development process to support the WINDMOOR 12 MW wind turbine on one of its columns, as illustrated in Fig. 1. The INO WINDMOOR substructure was initially designed as a semisubmersible wind turbine platform comprising three interconnected columns, supported by pontoons and deck beams.

The platform characteristics of the INO WINDMOOR have been detailed in Table 1.

Additionally, the mooring system of the INO WINDMOOR platform comprises three catenary lines, employing a combination of chain and polyester materials. The system is designed to maintain a pretension of 1050 kN, taking into account a water depth of 150 m. Further details regarding the characteristics of the WINDMOOR 12 MW wind turbine can be found in Table 2. This table provides a comprehensive overview of parameters including power output, rotor diameter, hub height, and

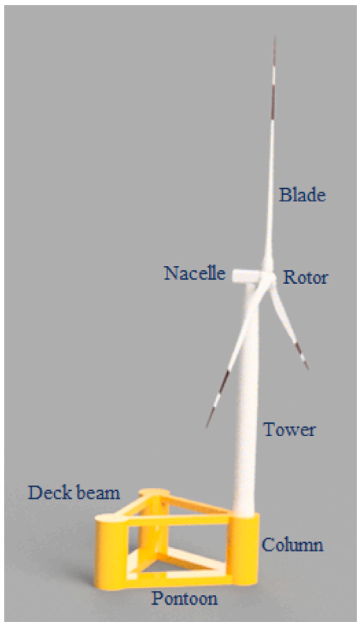

Fig. 1. Concept of WINDMOOR 12 MW floating wind turbine.

Table 1
Characteristics of the INO WINDMOOR substructure.

Property	Value
Column diameter	15 m
Column height	31 m
Pontoon width	10 m
Pontoon height	4 m
Center-center distance	61 m
Deck beam width	3.5 m
Deck beam height	3.5 m
Total substructure mass including ballast	12 058 t
Total substructure CGx[a]	−6.34 m
Total substructure CGy[a]	0 m
Total substructure CGz[a]	−10.03 m

[a] CG: Center of Gravity.

Table 2
Properties of the WINDMOOR 12 MW wind turbine.

Parameter	WINDMOOR 12 MW
Rated electrical power	12 MW
Specific power	324.8 W/m^2
Rotor orientation	Clockwise rotation - upwind
Number of blades	3
Rotor diameter	216.9 m
Hub diameter	5 m
Blade length	105.4 m
Blade prebend	6.8 m
Shaft tilt	6.0 deg
Rotor precone	−4.0 deg
Hub height	131.7 m
Cut-in/rated/cut-out wind speed	4.0/10.6/25.0 m/s
Generator efficiency	94.4%
Cut-in/rated rotor speed	5.5/7.8 rpm
Maximum tip speed	88.6 m/s
Blade mass	3 × 63 024 kg
Hub mass	60 000 kg
Nacelle mass	600 000 kg

other relevant specifications, offering insights into the specific features of the WINDMOOR 12 MW wind turbine.

The main properties of the tower are outlined in Table 3.

The substructure of the WINDMOOR 12 MW wind turbine has been modified to incorporate dual OWC systems while retaining the primary characteristics of the turbine, including the tower, blades, and Rotor-Nacelle Assembly (RNA). Fig. 2 illustrates the modifications made, wherein chambers have been created within the two columns of the substructure where the tower is not installed.

Table 3
Properties of the tower.

Parameter	Value
Diameter at top	5.97 m
Diameter at bottom	9.90 m
Thickness at top	30.1 mm
Thickness at bottom	90.0 mm
Length	110.20 m
Mass	1186.5 t
CG_z from base	56.65 m

The OWC systems installed in the modified WINDMOOR 12 MW wind turbine each consist of an air chamber connected to a turbine generator through a Power Take-Off (PTO) system [42]. These chambers feature openings below the waterline, enabling waves to enter and compress the air inside. The compressed air then drives the turbine, generating torque for the generator. As the wave water recedes, the air is drawn out in the opposite direction, but the turbine continues to rotate in the same direction due to its self-rectifying design. To minimize oscillations in the system, the OWCs' valves are responsible for controlling the compression and decompression of air within the air chambers. In Fig. 2, the setup of the throttle valve of the PTO system of the OWC is demonstrated.

However, in the present study, the throttle valves of the OWCs are intentionally kept open to evaluate the stability of the system without any control on the OWCs. This approach allows for an assessment of the system's behavior under uncontrolled operating conditions, enabling a better understanding of its inherent stability characteristics.

The OWCs in the hybrid system, as depicted in Fig. 2, are equipped with Wells turbines that share characteristics with the Mutriku power plant. These Wells turbines are vertically mounted directly above the capture chambers. The turbo-generator module associated with each Wells turbine is relatively compact, measuring approximately 2.83 m in height and having a maximum width of 1.25 m. Its weight is estimated to be around 1200 kg [43]. It is worth noting that in future studies, there is a possibility for further optimization of the Wells turbine size to ensure efficient energy harvesting from wave resources.

The substructure design has been conducted for the original FWT referred to as INO WINDMOOR, as illustrated in Fig. 3. Also, a hybrid semisubmersible FWT-OWCs with a chamber size of 4.5 m has been developed, as depicted in Fig. 4. The substructures in the study are constructed using steel material, characterized by ρ_{steel} = 7850 kg/m^3, E = 200 GPa. The detailed characteristics of the substructures for both platforms, including column, pontoon, and deck dimensions, have been comprehensively described in Table 1. Note that the reference point, in Figs. 3 and 4, is situated at the center of the platform (0 m, 0 m, 0 m).

To enhance the functionality of the INO WINDMOOR platform, modifications have been made to incorporate two chambers within its two columns. Consequently, the required ballast inside the columns for the hybrid system substructure was adjusted to effectively counterbalance the weight of the turbine, as illustrated in Fig. 4a. In order to conduct a sensitivity study, two additional cases have been considered, wherein the chamber size was set at 7.5 m (half of the column diameter) and 10 m (two-thirds of the column diameter). In the next sections, the impact of these variations in chamber size have been analyzed on the system's hydrostatic performance and behavior, thereby providing an assessment of its sensitivity to chamber dimensions.

Table 4 presents comprehensive information on the properties of the FWTs with and without OWCs. The table includes details such as the ballast properties, FWTs weight, and substructure weight for the analyzed systems.

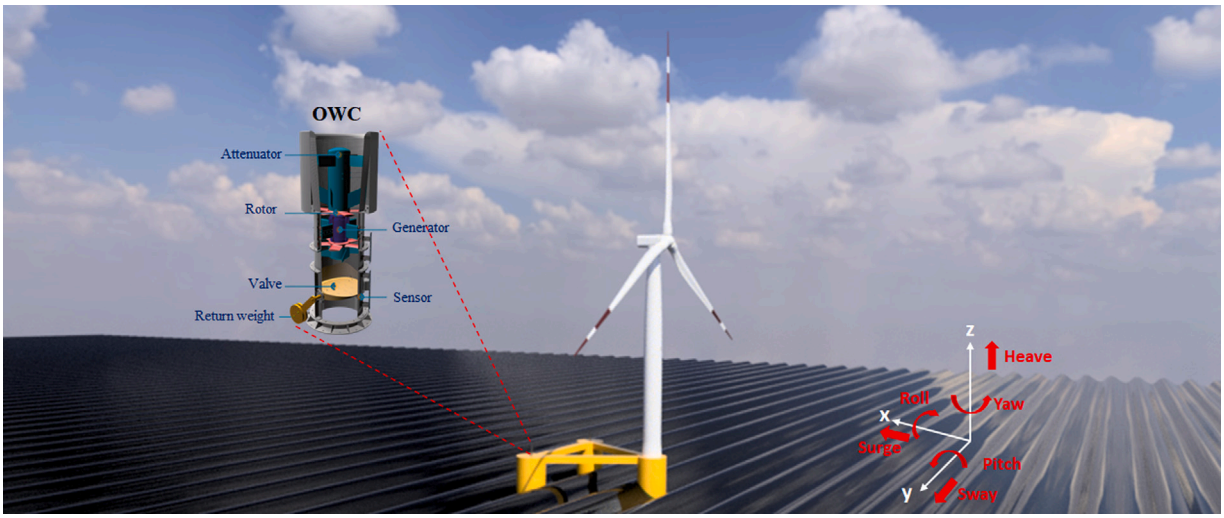

Fig. 2. Hybrid Semisubmersible FWT-OWCs.

Table 4
Full floating wind turbine properties.

Parameter	INO WINDMOOR	FWT-OWCs 1	FWT-OWCs 2	FWT-OWCs 3
Chamber size	No chamber	4.5 m	7.5 m	10 m
Ballast height	11.85 m	21.89 m	13.28 m	19.52 m
Substructure weight	12 058 t	10 806 t	9717 t	8615 t
Platform's center of gravity	−6.34, 0, −10.03 (m, m, m)	−6.14, 0, −8.93 (m, m, m)	−4.86, 0, −10.50 (m, m, m)	−3.22, 0, −10,14 (m, m, m)
Waterline Z	2.90 m	1.60 m	1.64 m	1.62 m
Substructure draft	18.40 m	17.10 m	17.14 m	17.12 m
Displaced volume	13 750 m^3	12 529 m^3	11 575 m^3	10 391 m^3
Volume loss	0%	8.88%	15.81%	24.42%
FWT system weight	14 094 t	12 842 t	11 864 t	10 650 t
FWT's center of gravity	0, 0, 4.03 (m, m, m)	0.78, 0, 6.32 (m, m, m)	2.29, 0, 6.40 (m, m, m)	4.56, 0, 8.48 (m, m, m)
Center of buoyancy	0, 0, −8.85 (m, m, m)	0.77, 0, −9.51 (m, m, m)	2.30, 0, −9.70 (m, m, m)	4.56, 0, −10.04 (m, m, m)

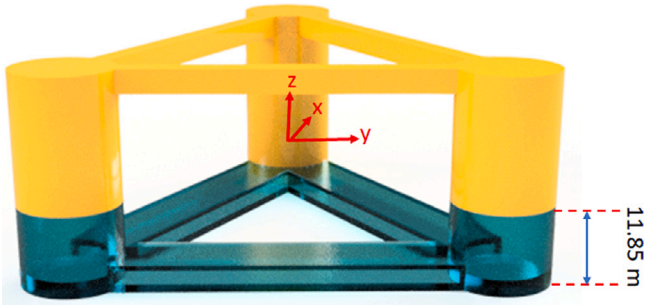

Fig. 3. Semisubmersible FWT's platform with the illustration of fixed ballast.

3. Equations of motion for FWTs

In order to ensure an accurate modeling that closely resembles the real behavior of FWTs, the equations of motion have been derived utilizing a frequency domain representation and the Morison Theory formulation. This approach enables a comprehensive analysis of the system's dynamic response to external forces and environmental conditions. In floating wind turbine design and operation, reference frames are employed to analyze and understand the system's behavior. The Earth-fixed frame serves as a global reference point, allowing precise measurement of the wind turbine's position and orientation in relation to the Earth's center. The body frame, attached to the wind turbine structure, streamlines the assessment of internal motions and structural responses by co-moving with the turbine itself. Additionally, the hydrodynamic frame is utilized to model how the wind turbine interacts with water and waves. In the frequency domain, the equation of motion for FWTs with respect to the hydrodynamic reference frame can be expressed as follows [34]:

$$I_{FWT}(\omega)\ \ddot{x}(\omega) + B_{FWT}(\omega)\ \dot{x}(\omega) + C_{FWT}\ x(\omega) = \vec{f}_{FWT}(\omega) \tag{1}$$

where the terms ω, I_{FWT}, B_{FWT}, and C_{FWT} represent the incident wave frequency, inertia, damping and restoring matrix of the FWT motions, respectively. These parameters have been linearized to simplify the analysis. The vector $\vec{f}_{FWT}(\omega)$ denotes the hydrodynamic forces, aerodynamic loads and power take off (PTO) force acting on the system. The variable x in Eq. (1) represents the platform motion as follows:

$$x = \begin{bmatrix} \text{surge} \\ \text{sway} \\ \text{heave} \\ \text{roll} \\ \text{pitch} \\ \text{yaw} \end{bmatrix} \tag{2}$$

The inertia matrix of the FWT motions can be described by:

$$I_{FWT}(\omega) = A_{Hydro}(\omega) + M_{FWT} \tag{3}$$

in the context of the equation, the term M_{FWT} represents the mass of the FWT system, encompassing all its structural components. It includes the mass of the tower, inclusive of the tower-top rotor-nacelle assembly

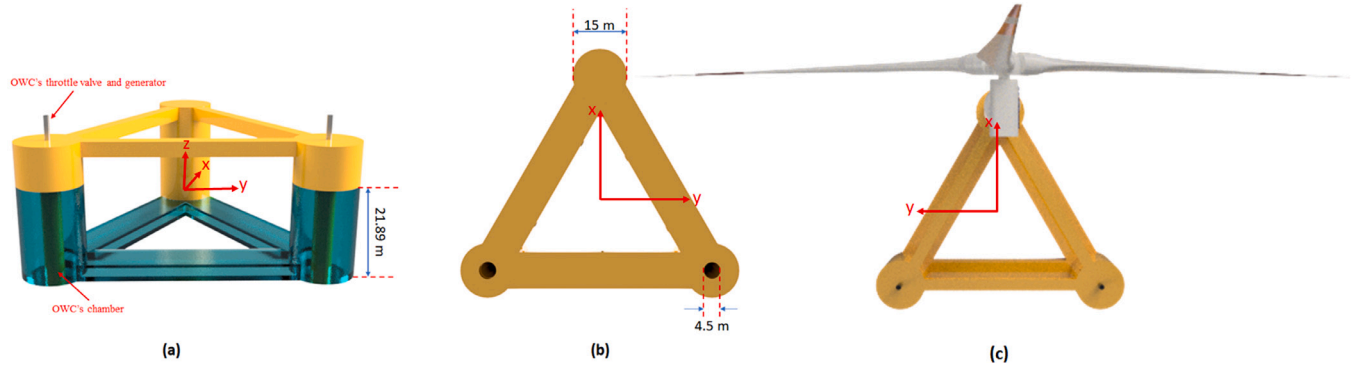

Fig. 4. Hybrid Semisubmersible FWT-OWCs with the illustration of fixed ballast for (a) front view. (b) bottom view. (c) top view.

(RNA), blades, substructure and OWC weight. Also, the platform's added mass is expressed as A_{Hydro}, which can be accurately determined using the panel radiation program WADAM [40].

The damping coefficients in the system can be expressed as follows:

$$B_{FWT}(\omega) = B_{Hydro}(\omega) + B_{vis} + B_{PTO} \tag{4}$$

where B_{Hydro} represents the damping elements of the platform derived from the radiation problem and includes the contributions from hydrodynamic effects and B_{vis} describes the viscous drag calculated from Morison Equation. B_{PTO} denotes the damping specific to the PTO mechanism of the OWCs.

The stiffness matrix C_{FWT} in Eq. (1) can be represented as follows:

$$C_{FWT} = C_{Hydro} + C_{Mooring} + C_{PTO} \tag{5}$$

where terms C_{Hydro}, $C_{Mooring}$ and C_{PTO} represent different components of the stiffness matrix C_{FWT}. C_{Hydro} accounts for the hydrostatic restoring matrix of the platform. C_{PTO} represents the stiffness associated with the PTO system in the OWCs. $C_{Mooring}$ relates to the stiffness elements associated with the mooring lines, which contribute to the platform's overall stiffness and play a role in maintaining its position. It is worth mentioning that in this article, the OWCs' valves have been kept open, leading to atmospheric air pressure inside the capture chambers. As a result, the PTO force, along with the parameters B_{PTO} and C_{PTO}, is negligible. The mooring system's linear restoring coefficient has been included as an external stiffness matrix in the analysis as follows:

$$C_{Mooring} = \begin{bmatrix} 89800\ \text{N/m} & 0 & 0 & 0 & 0 & 0 \\ 0 & 89800\ \text{N/m} & 0 & 0 & 0 & 0 \\ 0 & 0 & 0 & 0 & 0 & 0 \\ 0 & 0 & 0 & 0 & 0 & 0 \\ 0 & 0 & 0 & 0 & 0 & 0 \\ 0 & 0 & 0 & 0 & 0 & 1.2165e8\ \text{N m} \end{bmatrix} \tag{6}$$

Due to the dominant influence of hydrostatic stiffness in the semi-submersible platform configuration, the stiffness matrix elements have been neglected for heave, pitch, roll, and the surge-pitch and sway-roll coupling terms in Eq. (6).

To determine the added mass, damping coefficients, restoring matrix, and hydrodynamic force, a finite element model of the meshed platform was created and analyzed using the WADAM tool. The platform was discretized into mesh elements, with each element having a size of 0.75 m. This detailed mesh allowed for accurate calculations of the hydrodynamic properties and forces acting on the platform, enabling a comprehensive characterization of its dynamic behavior in the presence of waves and fluid interactions. Fig. 5a and b depict the meshed platforms for the WINDMOOR substructure and the substructure with OWC chambers. It is important to emphasize that although the complete substructures have been meshed, the WADAM analysis exclusively takes into account the wetted surfaces.

The WADAM tool utilizes the radiation and diffraction panel method to analyze the impact of unsteady hydrodynamic loads and motions on a body submerged in a fluid medium. By integrating pressures using the panel method and applying potential flow theory, WADAM provides a converged solution for diffraction and radiation phenomena occurring on the surface of the body.

Potential flow theory, which is employed by WADAM, assumes certain conditions, including an inviscid fluid (no internal friction), incompressible fluid (with constant density), and irrotational flow, assuming an ideal fluid. Hence, energy dissipation due to viscosity and turbulence is not considered in potential flow theory. While this theory is useful for many applications, it does not account for the effects of viscous damping that exists in real-world scenarios. As a result, potential flow theory tends to overestimate the resonant response of FWT structures.

To address this limitation, the Morison model has been considered in this study to incorporate the effects of viscous damping on the substructure. The Morison model introduces the influence of viscous damping by including drag forces on the substructure. By combining the results obtained from WADAM with the Morison model, a more comprehensive understanding of the system's dynamic behavior is achieved, accounting for the effects of viscous damping that potential flow theory overlooks.

Morison's representation combined with strip theory enables the straightforward computation of linear wave loads and nonlinear viscous-drag loads, particularly for slender vertical surface-piercing cylinders extending to the sea floor. Strip theory divides the structure into elements or strips, using two-dimensional properties to determine the overall three-dimensional loading on the structure. This approach provides an efficient and comprehensive method for calculating wave and drag loads on specified cylinders.

The general viscous drag force F_D from Morison equation can be expressed as follows:

$$F_D = \frac{1}{2}\rho\sigma C_D(v-\dot{x})|v-\dot{x}| = \frac{1}{2}\rho\sigma C_D\frac{8}{3\pi}V_{max}(v-\dot{x}) = B_{vis}(v-\dot{x}) \tag{7}$$

where the linearized viscous damping matrix $B_{vis} = \frac{1}{2}\rho\sigma C_D\frac{8}{3\pi}V_{max}$ is obtained from the linearization of F_D and used in Eq. (4). ρ, C_D and σ are the water density, drag coefficient matrix and projected area of the Morison element. Also, V_{max} is a linearized velocity amplitude specified as input to WADAM. v and $\dot{x}$ are the flow velocity and structure velocity, respectively. In the present study, the non-dimensional drag coefficients C_d presented in Table 5 have been obtained from DNV-RP-C205 [44].

Table 5
Quadratic drag coefficients for columns and pontoons.

	$C_{d,y}$	$C_{d,z}$
Column	1.0	1.0
Pontoon	2.3	1.4

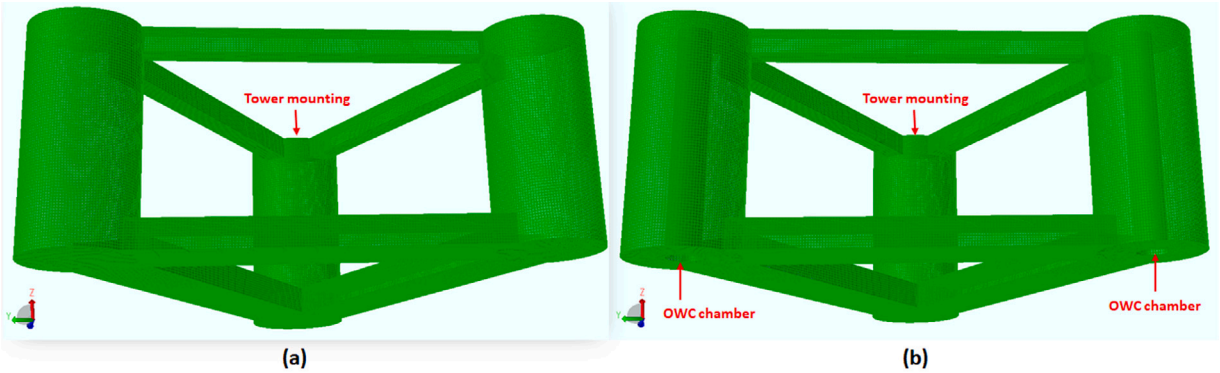

Fig. 5. Meshed platforms for (a) WINDMOOR substructure. (b) substructure with OWC chambers.

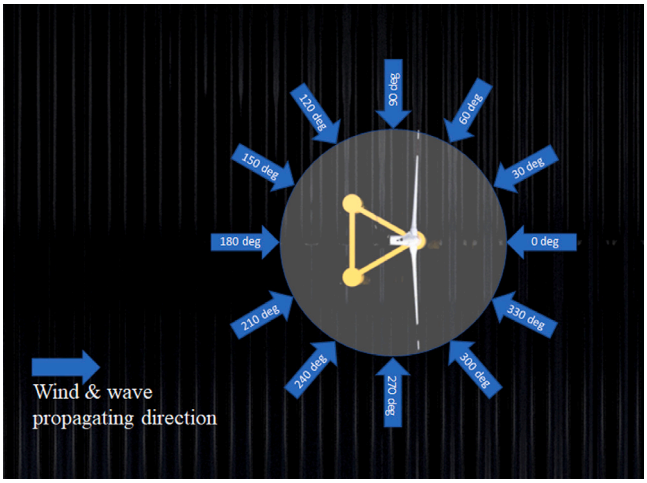

Fig. 6. Wind and wave propagating direction.

4. Hydrostatic stability analysis

In this section, a hydrostatic stability analysis has been conducted to assess the integrity of the FWT system. The evaluation of hydrostatic stability is based on the intact criteria, as specified by the Norwegian Maritime Authority (NMA) in the Regulations for Mobile Offshore Units (2003 Edition) - General Regulations V1-3-878/91-p20.

The assessment of intact hydrostatic stability holds significant importance in the design of offshore turbines, as it directly influences the FWT's ability to maintain its upright position under operational conditions. In other words, intact hydrostatic stability refers to the FWT's capacity to resist capsizing or tilting over due to external forces such as wind and waves. The wave and wind propagating direction of the FWT system are showed in Fig. 6.

The evaluation of the FWT's hydrostatic performance involves the assessment of both the righting moment and wind heeling moment. The righting moment determines the FWT's ability to maintain stability by counteracting external forces, while the wind heeling moment assesses the effect of wind on tilting the FWT.

To calculate the wind heeling moment, the thrust of the 12 MW wind turbine in different regions has been analyzed and plotted in Fig. 7. The figure showcases four distinct zones that have been taken into consideration. Zone I corresponds to the parked state of the turbine when there is insufficient wind power. Zone II represents wind speeds below the rated threshold, while Zone III encompasses wind speeds exceeding the rated limit. Finally, Zone IV represents the survival region, which corresponds to extreme wind conditions where the wind turbine is parked. In this zone, the turbine is designed to withstand severe wind speeds and is not actively generating power. Note that the calculated thrust has been obtained from the blades drag thrust including the tower drag impact. It is important to note that the calculated thrust presented in Fig. 7 includes the drag thrust generated by the blades as well as the impact of tower drag. The force exerted by the wind on the turbine blades as thrust, can be calculated as follows:

$$F_{Thrust} = \frac{1}{2}\rho A V^2 C_t \tag{8}$$

where ρ, A, V represent the density of the air, the effective swept area of the turbine and the mean wind velocity at hub height, respectively. C_t is the thrust coefficient, which characterizes the turbine's aerodynamic efficiency in converting wind energy into thrust force.

For components of the FWT above the waterline, such as the tower and nacelle, the wind pressure can be calculated by the following formula:

$$F_{\text{wind}} = \frac{1}{2}\rho C_s C_h A_{wind} V_{wind}^2 \tag{9}$$

where C_s and C_h represent the shape coefficient and the height coefficient, respectively. A_{wind} and V_{wind} express the projected area and the mean wind speed at a given elevation above the waterline, respectively. In the calculation of the wind load on the FWT above the waterline, it is assumed that the wind is constant and uniform.

The wind heeling moment, denoted as M_{wind}, can be calculated as follows:

$$M_{\text{wind}} = F_{\text{Thrust}}\,(z_{hub} - z_{COB})\,cos^2(\theta) + F_{\text{wind}}\,H_z \tag{10}$$

where F_{thrust} is the thrust force, as calculated using Eq. (8). z_{hub} and z_{CoB} are the hub height and center of buoyancy height, respectively. Additionally, θ is the heeling angle and H_z describes the distance from the wind pressure point to the center of buoyancy.

According to Eq. (10), the wind heeling moment curves are generated to illustrate the relationship between the wind heeling moment and the corresponding heel angle. Fig. 8 showcases these curves, depicting the wind heeling moment for various wind speeds. Assuming the wind field is constant and uniform, the selected wind speeds for which the wind heeling moment is plotted include:

- 11.25 m/s: This wind speed represents the scenario where the maximum thrust is imposed on the turbine.
- 10.6 m/s: Corresponding to the rated wind speed.
- 8 m/s: This wind speed lies below the rated wind speed.
- 16 m/s and 25 m/s: These wind speeds are above the rated wind speeds.
- 50 m/s: Denoting the survival condition, this wind speed represents the situation where the turbine is parked.

The wind heeling moment curve corresponding to a wind speed of 11.25 m/s, represented by the black dot–dash line in Fig. 8, exhibits the maximum overturning moment. This particular curve is of significant

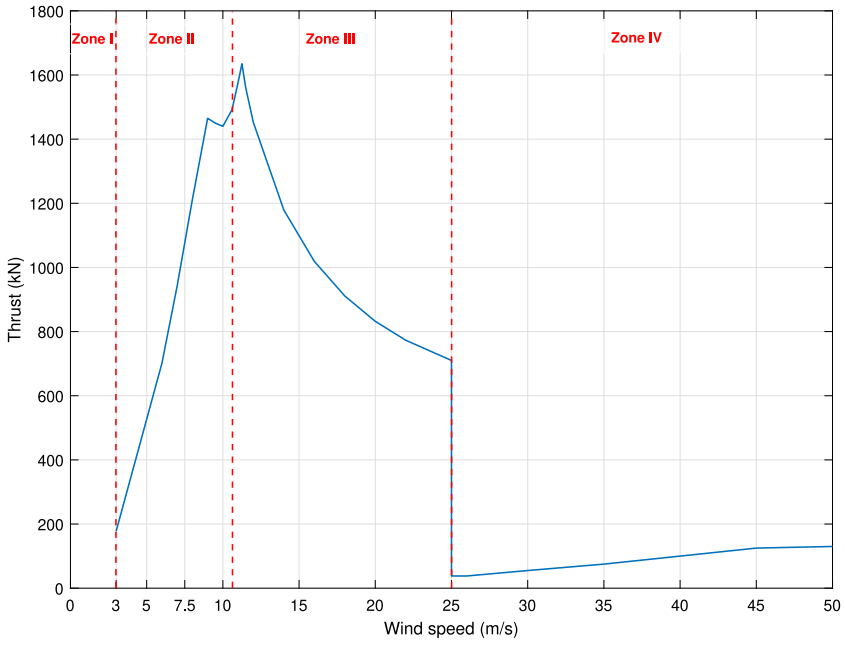

Fig. 7. Thrust.

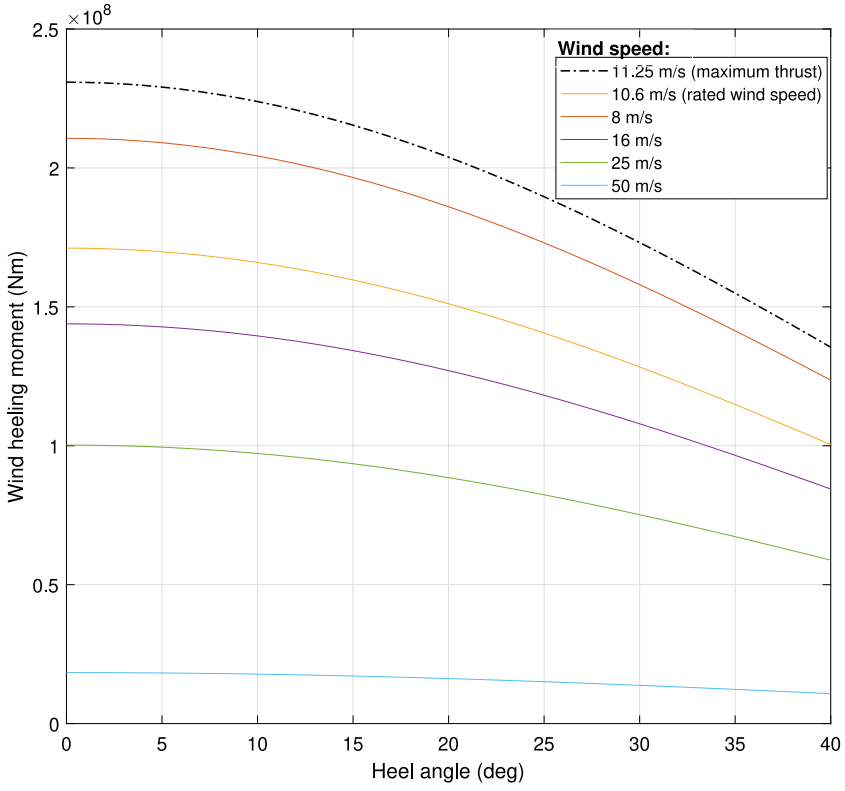

Fig. 8. Wind heeling moment for selected wind speeds.

importance as it represents the most severe wind heeling moment case that can occur for the 12 MW wind turbine. Due to the significance and severity of this curve, it has been selected to be included in the hydrostatic evaluation of the FWTs.

As a considered restriction on the heel angle, it is assumed that the tower and OWCs' wells turbine are not water-proof, necessitating measures to prevent water from reaching the top of the substructure as the heeling angle increases. Fig. 9 provides three visual representations. The first captures the equilibrium at 0° heel angle, while the second reveals a 15° heel angle around the 270° rotation axis, marking point A's submersion inception. Lastly, the third shows a 15° heel angle around rotation axis of 90°, as point B starts to be submerged.

Fig. 10 illustrates the relationship between the righting moments and wind heeling moment as a function of heeling angle for the

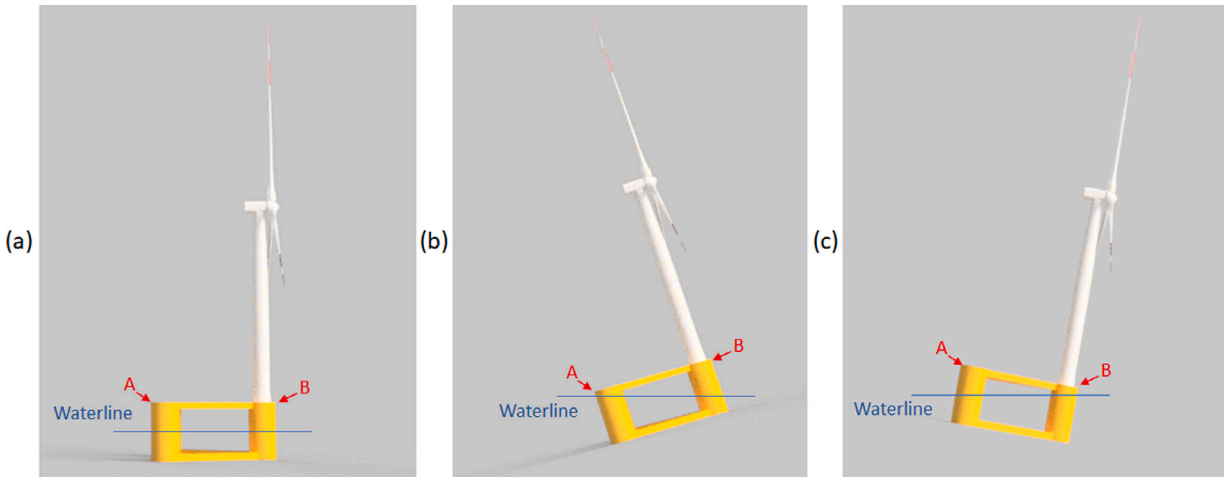

Fig. 9. Waterline representation. (a) FWT with the heel angle of 0 deg. (b) FWT with the heel angle of 15 deg for the rotation axis of 270 deg. (c) FWT with the heel angle of 15 deg for the rotation axis of 90 deg.

WINDMOOR 12 MW FWT. Additionally, Figs. 11, 12, and 13 present the designed hybrid FWT-OWCs systems with chamber sizes of 4.5 m, 7.5 m, and 10 m, respectively.

The overturning moment experienced by the wind turbine has been calculated based on the maximum thrust and is represented as the wind heeling moment in the figures using a dot-dash black line.

As observed in Figs. 10, 11, 12, and 13, the righting moments are plotted with respect to the rotation axis, ranging from −90° to 90° at 15° intervals, while considering the heel angle from 0° to 40°. In the stable cases depicted in Figs. 10, 11, and 12, the righting moment is zero at a heel angle of 0°, indicating an alignment of the buoyant force and the FWT's weight, resulting in no moment being generated. As the heel angle increases, the righting moment steadily rises until it reaches its peak value. Beyond this peak righting moment, as the heel angle further increases, the righting moment gradually diminishes, putting the FWT at risk of capsizing. At the point of peak righting moment, the FWT generates its maximum internal moment in response to the external moment created by external forces. However, if the external moment exceeds the internal moment, the FWT will continue to heel over until it capsizes, reaching a righting moment of 0° again. This critical point is known as the "turning point" or the "angle of vanishing stability". At the turning point, no internal moment couple is present, and the FWT becomes capsized, unable to self-right.

As evident from the plotted righting moment curves, such as those in Fig. 10 for the original FWT and Fig. 11 for the FWT-OWCs with an air chamber of 4.5 m, certain rotation angles exhibit an "angle of vanishing stability" that exceeds 40°. This means that for specific rotation axes, such as 30° and 270° for the original FWT and 30°, 45°, and 270° for the FWT-OWCs, the FWT is capable of maintaining stability at heeling angles beyond 40°. However, there are cases, like the 285° rotation axis for both FWTs, where the "angle of vanishing stability" is approximately 30°.

Concerning the righting moments with different rotation axes depicted in Figs. 10, 11, 12, and 13, it is noteworthy that the rotation axis attributed to the righting moment (270 deg) finds its visual correlation in Fig. 9b. In this depiction, the heeling angle stands at 15°. Additionally, Fig. 9c offers a visual representation that aligns with the rotation axis of 90°, accompanied by a 15° heeling angle.

To assess the hydrostatic stability of the systems, the intact stability rules set by the Norwegian Maritime Authority (NMA) have been taken into account. Five criteria have been carefully evaluated to ensure intact static stability.

The first criterion stipulates that the equilibrium inclination angle with the wind should not exceed 17 degrees. The second criterion states that the second intercept of the righting/heeling moment should exceed 30 degrees. This intercept occurs where the wind heeling moment crosses the righting moment.

The third criterion requires the righting moment curve to be positive over the entire range of angles from the upright position to the second intercept. The fourth criterion specifies that the metacentric height in equilibrium must be greater than 1 m.

Lastly, for column-stabilized units, the fifth criterion mandates that the area under the righting moment curve up to the angle of downflooding should be at least 30% greater than the area under the wind heeling moment curve up to the same limiting angle. These criteria collectively ensure the intact static stability of the FWT systems.

Also, the intact stability criteria have been summarized in Table 6 for INO WINDMOOR, Table 7 for the hybrid system with a chamber size of 4.5 m, and Table 8 for the hybrid system with a chamber size of 7.5 m. However, due to the observation in Fig. 13 that almost all of the criteria are not fulfilled, it is deemed unnecessary to provide a detailed table.

Nonetheless, the intact stability criteria regarding NMA rules [45] in the tables can be summarized as follows:

- Criterion 1: Equilibrium inclination angle with wind must not exceed maximum inclination (17 deg.).
- Criterion 2: The second righting/heeling moment intercept should be greater than the minimum second intercept (30 deg.).
- Criterion 3: The righting moment curve should be positive over the entire range of angles from upright to the second intercept.
- Criterion 4: The initial metacentric height (metacentric height in equilibrium) should be greater than or equal to the minimum GM.
- Criterion 5: The righting moment area to the minimum of second intercept and downflooding angle should exceed the heeling moment area by a margin set for the designated unit type.

It can be observed from Tables 6 and 7 that the hydrostatic stability of the original INO WINDMOOR FWT and the designed FWT-OWCs with a chamber size of 4.5 m have been ensured, considering different rotation axes for the righting moment and maximum wind heeling moment. However, as the chamber size increases to 7.5 m (refer to Table 8), some of the criteria are not met, indicating a decrease in stability. This situation worsens when the chamber size further increases to 10 m, rendering the system unstable. In such cases, the substructure can be modified to increase the draft by adjusting the diameter or height of the substructure columns.

5. Hydrodynamic analysis

Once the hydrostatic stability of the system has been ensured, the next step is to perform a hydrodynamic analysis to evaluate the system's

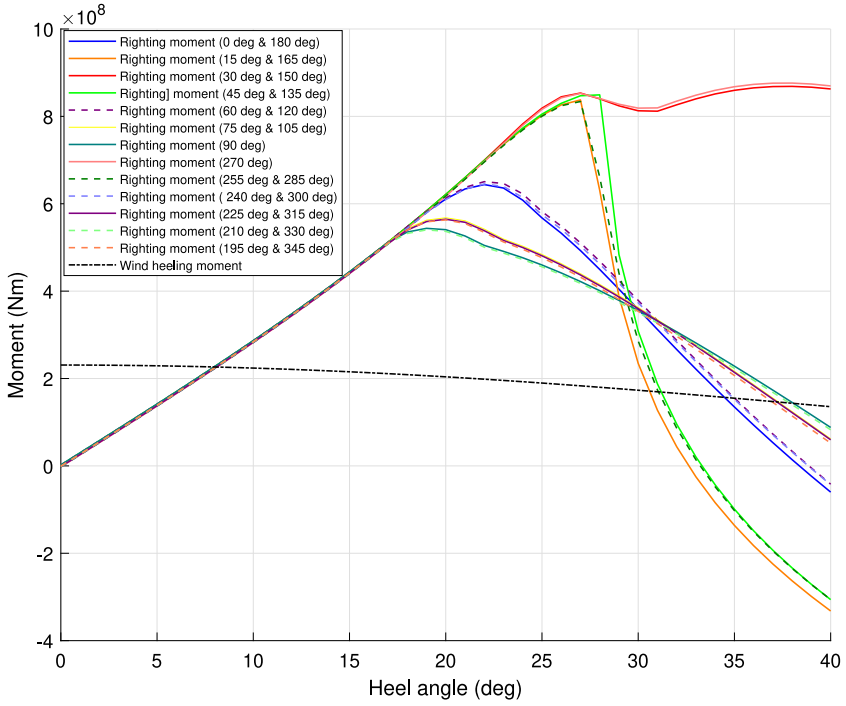

Fig. 10. Righting moment and wind heeling moment with respect to heel angle for FWT without OWCs.

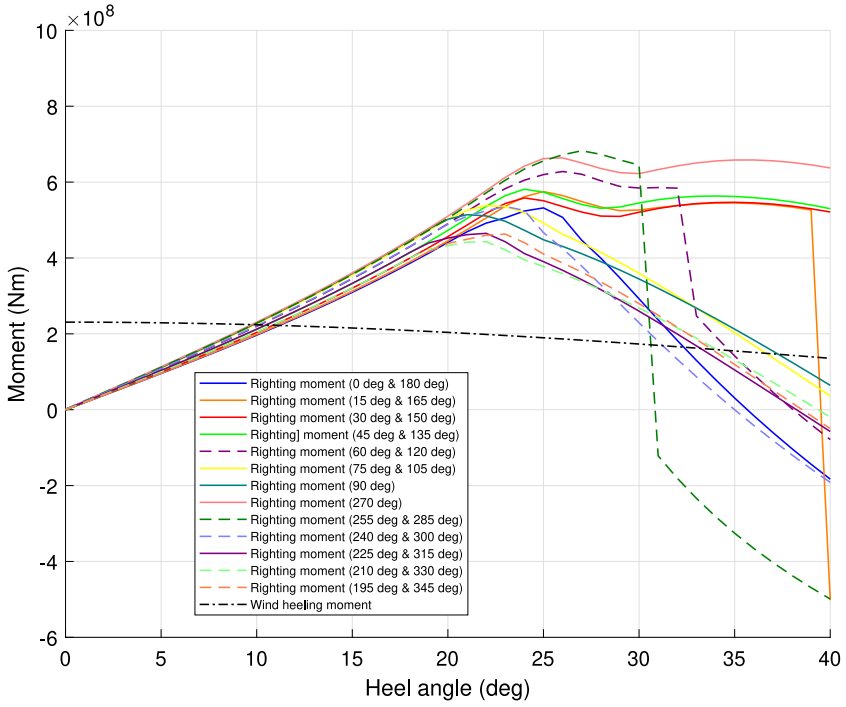

Fig. 11. Righting moments and wind heeling moment with respect to heel angle for hybrid FWT-OWCs with OWCs chamber of 4.5 m.

behavior when subjected to waves with different periods. This analysis involves studying the RAOs to assess the system's response to wave-induced forces and motions. The motion frequency-dependent RAOs for the six degrees of freedom, which include surge, sway, heave, roll, pitch, and yaw can be calculated. From Eq. (1) and considering $\vec{f}_{FWT}(\omega) = \xi_j F_j(\omega) e^{i\omega t}$, the following equation can be obtained:

$$(-\omega^2 I_{FWT} + i\omega B_{FWT} + C_{FWT}) X(\omega) e^{i\omega t} = \xi_j F_j(\omega) e^{i\omega t} \tag{11}$$

where $X(\omega)$ is the motion response at frequency ω and ξ_j is the wave amplitude of the jth mode of motion. Hence, the RAOs can be achieved as follows [46]:

$$RAO(\omega) = \frac{X(\omega)}{\xi_j} = \frac{F_j(\omega)}{-\omega^2 I_{FWT} + i\omega B_{FWT} + C_{FWT}} \tag{12}$$

The hydrodynamic analysis of the FWT-OWCs with chamber sizes of 7.5 m and 10 m has been deferred, as these systems require modifications to ensure their hydrostatic stability first.

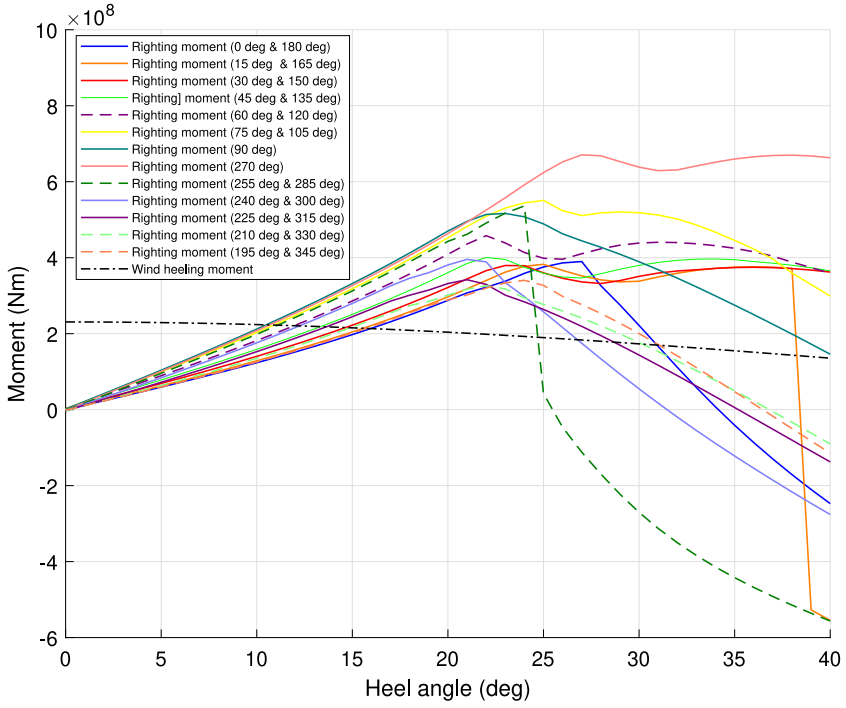

Fig. 12. Righting moments and wind heeling moment with respect to heel angle for hybrid FWT-OWCs with OWCs chamber of 7.5 m.

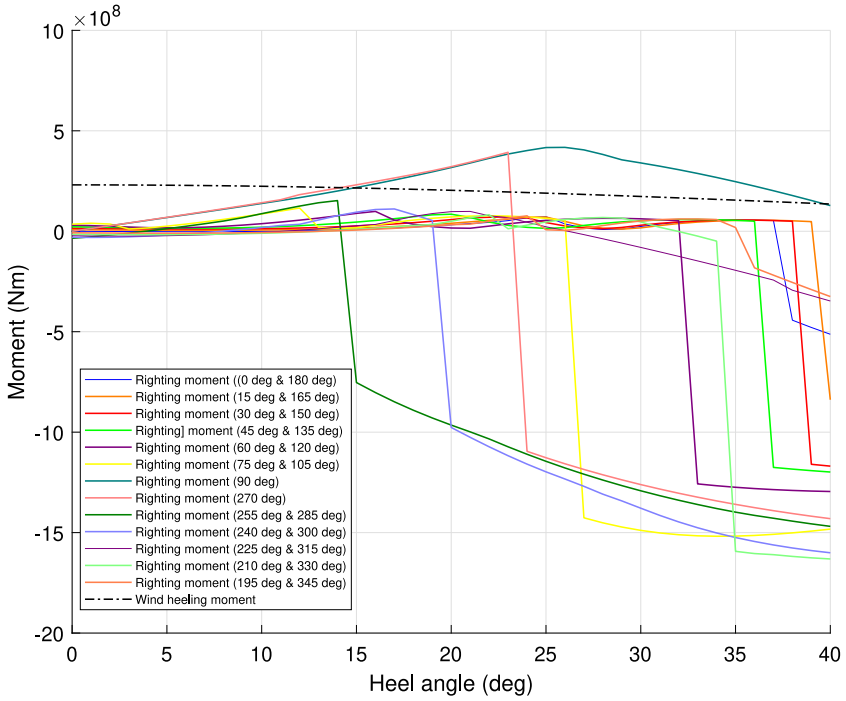

Fig. 13. Righting moments and wind heeling moment with respect to heel angle for hybrid FWT-OWCs with OWCs chamber of 10 m.

The RAOs for surge, sway, heave, roll, pitch, and yaw have been plotted in Figs. 14, 15, 16, 17, 18, and 19, respectively. The figures compare two cases: the redesigned WINDMOOR FWT without OWCs (a) and the hybrid FWT-OWCs with a chamber size of 4.5 m (b). The RAOs are shown for wave directions ranging from 0° to 180° in increments of 30°. One significant observation, as depicted in the figures and described in Table 9, is that the natural periods for certain modes, notably roll and pitch, have been shifted forward by approximately 3 s for the hybrid FWT-OWCs in comparison to the WINDMOOR FWT.

Figs. 14 and 15 demonstrate that as the wave period increases, the surge RAO and sway RAO, respectively, also increase. However, the figures indicate negligible differences between the hybrid FWT-OWCs and the WINDMOOR FWT. Note that the natural period for these modes of the systems are greater than 100 s.

Fig. 16 reveals that as the wave period increases, the heave RAOs also increase for both the WINDMOOR FWT and hybrid FWT-OWCs. For long wave periods, the heave RAO for both systems reaches 1 m/m, indicating that the heave motion closely follows the wave oscillations. A notable observation is the significant reduction in the heave RAO

Table 6
Hydrostatic properties for INO WINDMOOR.

Parameter	270	255	240	225	210	195	0	15	30	45	60	75	90
Criterion 1	8.22 ≤ 17 Pass	8.22 ≤ 17 Pass	8.21 ≤ 17 Pass	8.19 ≤ 17 Pass	8.17 ≤ 17 Pass	8.15 ≤ 17 Pass	8.13 ≤ 17 Pass	8.11 ≤ 17 Pass	8.09 ≤ 17 Pass	8.08 ≤ 17 Pass	8.07 ≤ 17 Pass	8.07 ≤ 17 Pass	8.06 ≤ 17 Pass
Criterion 2	∞ > 30 Pass	30.63 > 30 Pass	33.62 > 30 Pass	35.13 > 30 Pass	35.50 > 30 Pass	34.89 > 30 Pass	33.21 > 30 Pass	30.18 > 30 Pass	∞ > 30 Pass	30.77 > 30 Pass	33.70 > 30 Pass	35.22 > 30 Pass	35.70 > 30 Pass
Criterion 3	True Pass	True Pass	True Pass	True Pass	True Pass	True Pass	True Pass	True Pass	True Pass	True Pass	True Pass	True Pass	True Pass
Criterion 4	11.52 ≥ 1 Pass	11.52 ≥ 1 Pass	11.52 ≥ 1 Pass	11.52 ≥ 1 Pass	11.52 ≥ 1 Pass	11.52 ≥ 1 Pass	11.52 ≥ 1 Pass	11.52 ≥ 1 Pass	11.52 ≥ 1 Pass	11.52 ≥ 1 Pass	11.52 ≥ 1 Pass	11.52 ≥ 1 Pass	11.52 ≥ 1 Pass
Criterion 5	3.8e8 > 2.0e8 Pass	2.2e8 > 1.5e8 Pass	2.1e8 > 1.7e8 Pass	2.0e8 > 1.7e8 Pass	2.0e8 > 1.7e8 Pass	2.0e8 ≥ 1.7e8 Pass	2.1e8 > 1.6e8 Pass	2.2e8 > 1.5e8 Pass	3.8e8 > 2.0e8 Pass	2.3e8 > 1.5e8 Pass	2.1e8 ≥ 1.7e8 Pass	2.1e8 > 1.7e8 Pass	2.0 > 1.8e8 Pass

Table 7
Hydrostatic properties for hybrid FWT-OWCs with chamber size of 4.5 m.

Parameter	270	255	240	225	210	195	0	15	30	45	60	75	90
Criterion 1	9.72 ≤ 17 Pass	9.83 ≤ 17 Pass	10.10 ≤ 17 Pass	10.46 ≤ 17 Pass	10.82 ≤ 17 Pass	11.08 ≤ 17 Pass	11.18 ≤ 17 Pass	11.09 ≤ 17 Pass	10.85 ≤ 17 Pass	10.50 ≤ 17 Pass	10.16 ≤ 17 Pass	9.90 ≤ 17 Pass	9.81 ≤ 17 Pass
Criterion 2	∞ > 30 Pass	30.61 > 30 Pass	31.24 > 30 Pass	33.21 > 30 Pass	34.06 > 30 Pass	33.78 > 30 Pass	32.33 > 30 Pass	39.37 > 30 Pass	∞ > 30 Pass	∞ > 30 Pass	34.72 > 30 Pass	36.64 > 30 Pass	37.28 > 30 Pass
Criterion 3	True Pass	True Pass	True Pass	True Pass	True Pass	True Pass	True Pass	True Pass	True Pass	True Pass	True Pass	True Pass	True Pass
Criterion 4	8.63 ≥ 1 Pass	8.63 ≥ 1 Pass	8.63 ≥ 1 Pass	8.63 ≥ 1 Pass	8.63 ≥ 1 Pass	8.63 ≥ 1 Pass	8.63 ≥ 1 Pass	8.63 ≥ 1 Pass	8.63 ≥ 1 Pass	8.63 ≥ 1 Pass	8.63 ≥ 1 Pass	8.63 ≥ 1 Pass	8.63 ≥ 1 Pass
Criterion 5	3.0e8 > 1.7e8 Pass	1.9e8 > 1.4e8 Pass	1.5e8 > 1.4e8 Pass	1.5e8 > 1.5e8 Pass	1.5e8 > 1.5e8 Pass	1.5e8 ≥ 1.5e8 Pass	1.6e8 > 1.5e8 Pass	2.5e8 > 1.7e8 Pass	2.5e8 > 1.7e8 Pass	2.6e8 > 1.7e8 Pass	2.1e8 ≥ 1.6e8 Pass	1.9e8 > 1.6e8 Pass	1.9 > 1.6e8 Pass

Table 8
Hydrostatic properties for hybrid FWT-OWCs with chamber size of 7.5 m.

Parameter	270	255	240	225	210	195	0	15	30	45	60	75	90
Criterion 1	7.91 ≤ 17 Pass	10.33 ≤ 17 Pass	11.43 ≤ 17 Pass	12.79 ≤ 17 Pass	14.01 ≤ 17 Pass	14.81 ≤ 17 Pass	15.04 ≤ 17 Pass	14.65 ≤ 17 Pass	13.74 ≤ 17 Pass	12.47 ≤ 17 Pass	11.15 ≤ 17 Pass	10.13 ≤ 17 Pass	9.75 ≤ 17 Pass
Criterion 2	∞ > 30 Pass	24.73 > 30 Fail	27.15 > 30 Fail	29.30 > 30 Fail	30.83 > 30 Pass	31.56 > 30 Pass	31.19 > 30 Pass	38.26 > 30 Pass	∞ > 30 Pass	∞ > 30 Pass	∞ > 30 Pass	∞ > 30 Pass	∞ > 30 Pass
Criterion 3	True Pass	True Pass	True Pass	True Pass	True Pass	True Pass	True Pass	True Pass	True Pass	True Pass	True Pass	True Pass	True Pass
Criterion 4	5.78 ≥ 1 Pass	5.78 ≥ 1 Pass	5.78 ≥ 1 Pass	5.78 ≥ 1 Pass	5.78 ≥ 1 Pass	5.78 ≥ 1 Pass	5.78 ≥ 1 Pass	5.78 ≥ 1 Pass	5.78 ≥ 1 Pass	5.78 ≥ 1 Pass	5.78 ≥ 1 Pass	5.78 ≥ 1 Pass	5.78 ≥ 1 Pass
Criterion 5	2.9e8 > 1.6e8 Pass	1.1e8 > 1.1e8 Pass	1.0e8 > 1.2e8 Fail	9.8e7 > 1.2e8 Fail	9.8e7 > 1.3e8 Fail	1.0e8 > 1.3e8 Fail	1.0e8 > 1.3e8 Fail	1.6e8 > 1.5e8 Pass	1.7e8 > 1.6e8 Pass	1.9e8 > 1.6e8 Pass	2.1e8 > 1.6e8 Pass	2.3e8 > 1.6e8 Pass	2.0 > 1.6e8 Pass

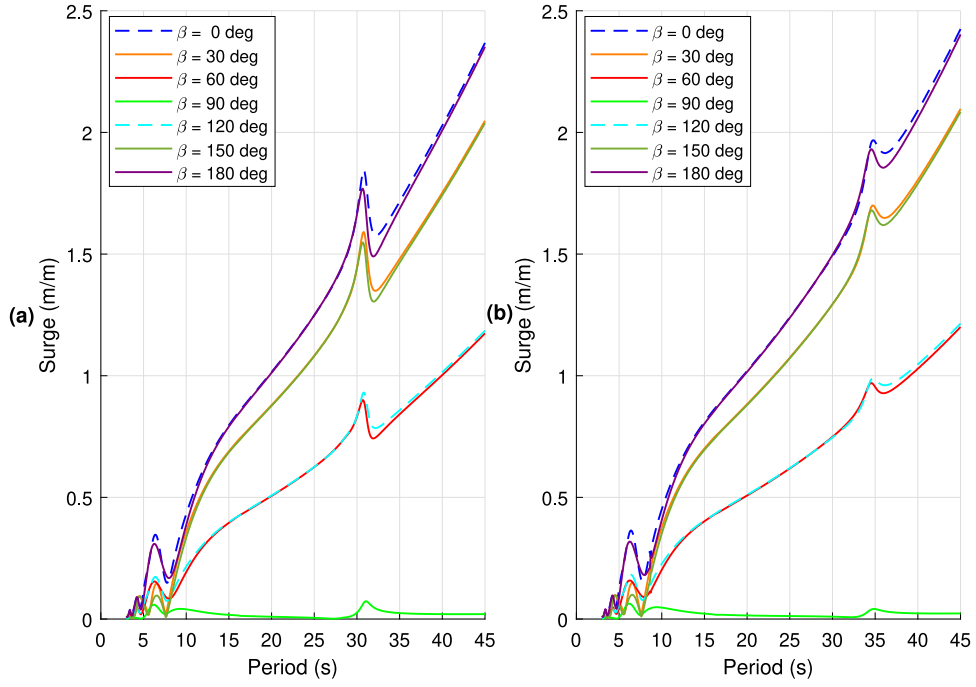

Fig. 14. Surge RAOs for (a) FWT without OWCs. (b) Hybrid FWT-OWCs.

amplitude at the natural period of 16.5 s, indicating a conciliation effect due to the presence of OWCs in the hybrid system compared to the WINDMOOR FWT. Moreover, minor peak variations in the RAO can be observed for the hybrid system around a wave period of 35 s, as depicted in Fig. 16b. These variations suggest a coupling between heave and pitch in the hybrid FWT-OWCs system. These findings suggest that the hybrid FWT-OWCs exhibit improved heave performance and reduced vibrations compared to the WINDMOOR FWT.

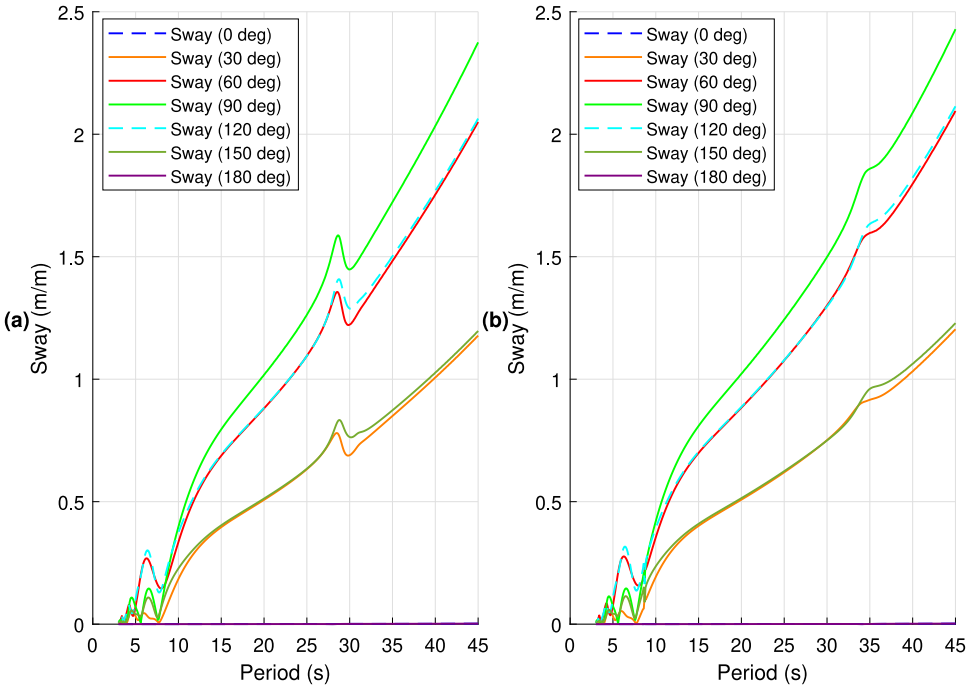

Fig. 15. Sway RAOs for (a) FWT without OWCs. (b) Hybrid FWT-OWCs.

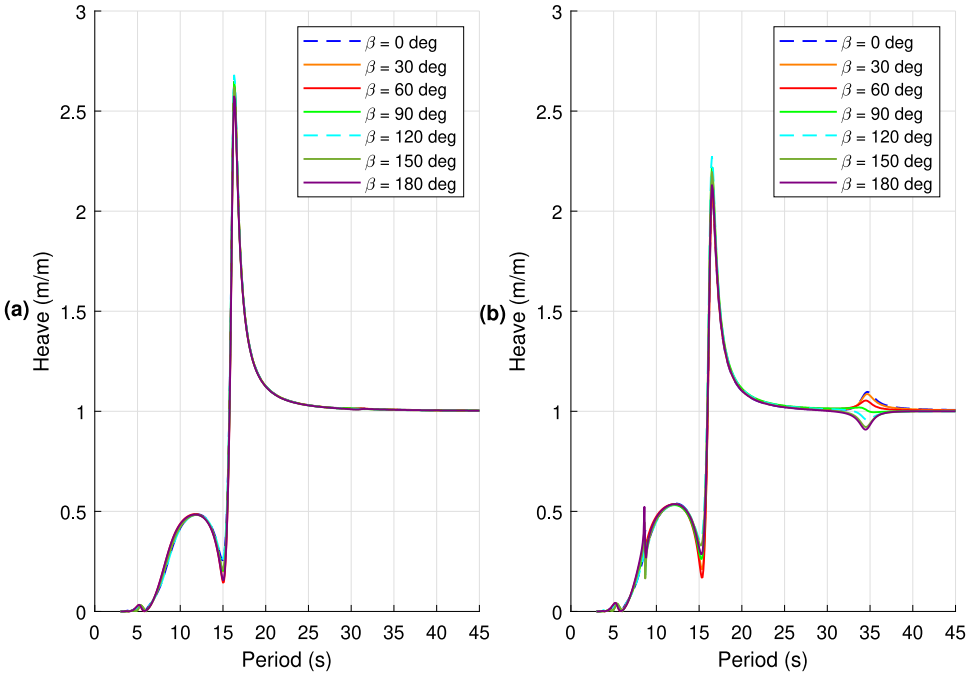

Fig. 16. Heave RAOs for (a) FWT without OWCs. (b) Hybrid FWT-OWCs.

Fig. 17 displays the roll RAOs for the WINDMOOR FWT and hybrid FWT-OWCs, indicating natural periods at 27.9 s and 32.6 s, respectively. A significant reduction in the roll RAO can be observed at the natural period for the hybrid system compared to the WINDMOOR FWT, highlighting the positive influence of the OWCs on roll motion mitigation. Additionally, the wave direction has a noticeable impact on the roll RAO. Specifically, wave directions of 0° and 180° result in the least roll RAO, while a wave direction of 90° induces the highest roll response. Furthermore, the zoomed-in view of the roll RAOs between periods of 5 s to 20 s reveals small changes for both systems, as the oscillations remain relatively low during this period.

One of the most crucial aspects in this study is the pitch angle, which plays a significant role in wind energy harvesting. In Fig. 18, the pitch resonant period for the WINDMOOR FWT is found at 30.9 s, while for the hybrid FWT-OWCs, it is at 34.6 s. It is evident that the hybrid system exhibits a substantial reduction in pitch resonant amplitude compared to the WINDMOOR FWT. Moreover, when focusing on the period between 5 s and 20 s, both systems demonstrate a low pitch RAO with negligible differences. Additionally, as the wave direction varies from 0° to 90°, the platform pitch decreases, indicating that this mode is less provoked by the incoming waves.

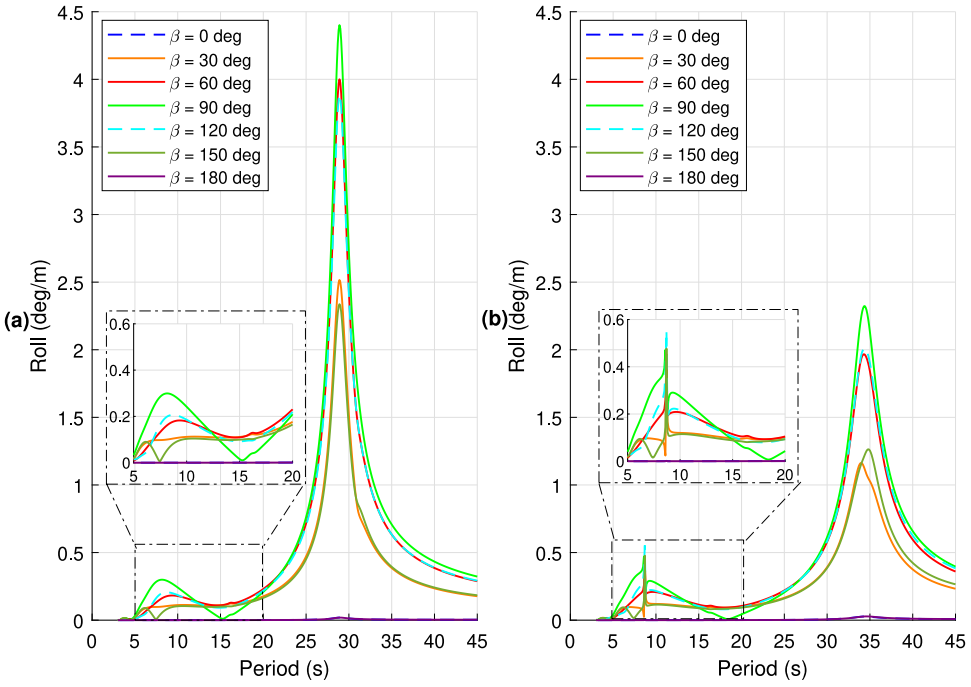

Fig. 17. Roll RAOs for (a) FWT without OWCs. (b) Hybrid FWT-OWCs.

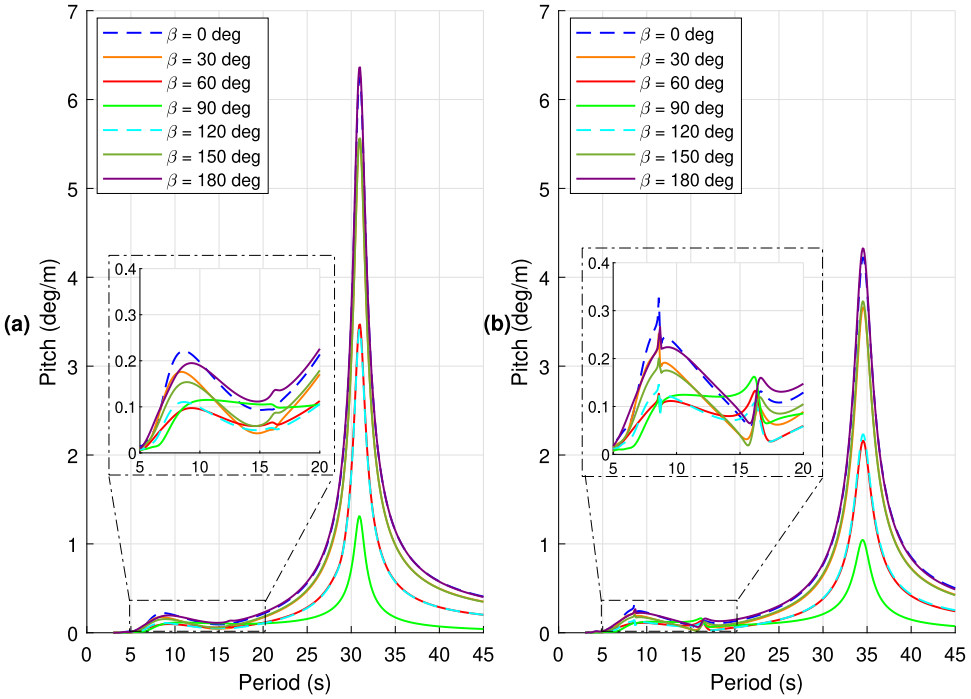

Fig. 18. Pitch RAOs for (a) FWT without OWCs. (b) Hybrid FWT-OWCs.

In comparison to other modes, the yaw angle, as depicted in Fig. 19, shows relatively lesser activation response, with the highest value occurring during the wave direction of 90°. The positive impact of the OWCs is noticeable in the yaw angle at a period of approximately 34 s for the hybrid system, when compared to the WINDMOOR FWT. It is worth noting that the yaw resonant period for both systems occurs at wave periods greater than 100 s. In addition, from the figures, a coupling between yaw and roll is observable for both FWT without OWCs and hybrid FWT-OWCs.

6. Conclusion and future work

This article presents an investigation into the integration of OWCs inside the submersible substructure of the INO WINDMOOR FWT. The FWTs design approach involves adjusting the ballast inside the FWT's columns to achieve proper balance and counteract the weight of the tower, RNA, and blades. The study encompasses hydrostatic stability and hydrodynamic analyses to evaluate the feasibility and performance of the integrated system.

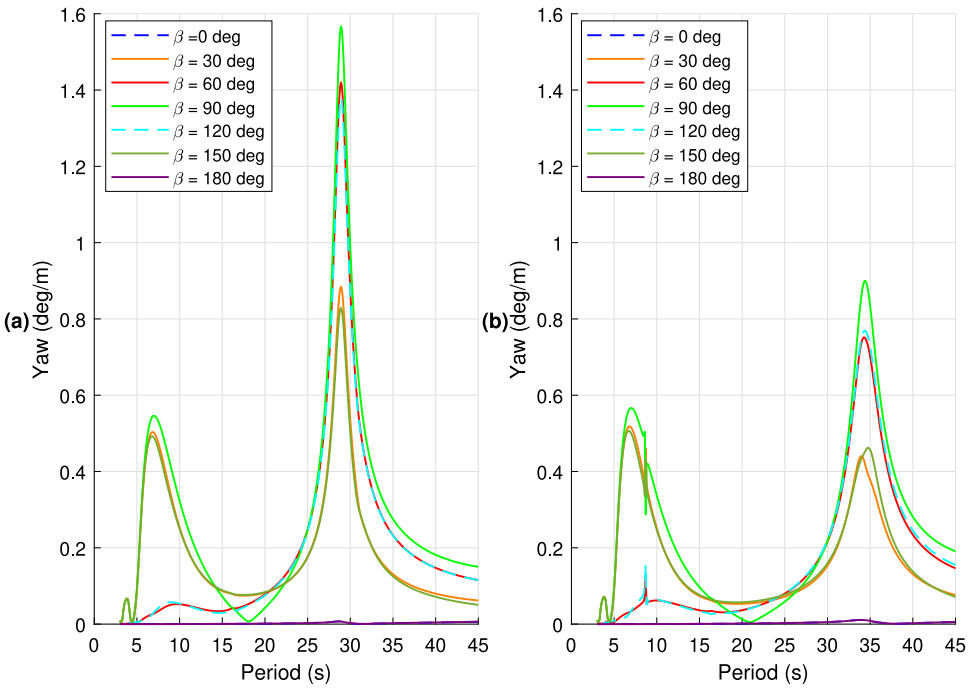

Fig. 19. Yaw RAOs for (a) FWT without OWCs. (b) Hybrid FWT-OWCs.

Table 9
FWTs natural periods.

Parameter	INO WINDMOOR	FWT-OWCs with chamber size of 4.5 m
Surge	105.4 s	101.8 s
Sway	105.2 s	101.4 s
Heave	16.4 s	16.5 s
Roll	27.9 s	32.6 s
Pitch	30.9 s	34.6 s
Yaw	113.2 s	132.1 s

In the hydrostatic stability analysis, the original WINDMOOR FWT and the FWT-OWCs with a chamber size of 4.5 m were examined. Results demonstrated that these configurations met all the criteria for intact hydrostatic stability. However, as the chamber size increased, certain criteria were not satisfied, indicating the need for substructure modifications to enhance stability by increasing the draft.

The hydrodynamic analysis focused on the WINDMOOR FWT and the FWT-OWCs with a chamber size of 4.5 m. The findings revealed that the inclusion of OWCs' chambers resulted in a reduction of resonant amplitudes for heave, roll, and pitch motions. This positive effect demonstrates the potential of the OWCs to mitigate oscillations in these states. Additionally, the presence of the OWCs resulted in a positive effect on pitch and roll responses, causing a shift in resonant period by approximately 5 s, which helps avoid resonance-related issues and improves overall stability and safety of the hybrid system.

Future work will include a promising direction to explore the implementation of a controller to emulate the functionality of the OWCs' valves. By utilizing active control methods in the time domain, the air flow can be actively regulated, leading to effective reduction of system oscillations. This approach has the potential to significantly enhance the performance and stability of the integrated FWT-OWCs system. The controller can be designed to respond to real-time environmental conditions, such as wave characteristics and wind speeds, enabling optimized operation of the OWCs and maximizing the overall performance of the hybrid FWT. Notably, the study did not consider the impact of wind load as the OWCs can positively affect the reduction of vibration caused by wind. Additionally, further exploration can be conducted to harness the energy from both waves using OWCs' wells turbine and wind from the wind turbine. This would involve studying the potential synergies and interaction effects between the two energy sources, aiming for a more comprehensive and integrated renewable energy system.

CRediT authorship contribution statement

Payam Aboutalebi: Conceptualization, Investigation, Methodology, Software, Writing – review & editing. **Aitor J. Garrido:** Conceptualization, Investigation, Methodology, Software, Writing – review & editing. **Izaskun Garrido:** Conceptualization, Investigation, Methodology, Software, Writing – review & editing. **Dong Trong Nguyen:** Conceptualization, Investigation, Methodology, Software, Writing – review & editing. **Zhen Gao:** Conceptualization, Investigation, Methodology, Software, Writing – review & editing.

Declaration of competing interest

The authors declare that they have no known competing financial interests or personal relationships that could have appeared to influence the work reported in this paper.

Acknowledgments

Funding

This work was supported in part by MICIN through PID2021-123543OB-C21 and PID2021-123543OB-C22 funded by MCIN/AEI/10.13039/501100011033, Basque Government through IT1555-22, and Margarita Salas grant MARSA22/09 by the European Union-Next Generation EU.

Appendix A. Panel size sensitivity study

Fig. 20 illustrates the RAOs for different configurations of the hybrid FWT-OWCs, featuring a 4.5 m chamber size. These RAOs are computed using three different mesh sizes: 1.5 m, 0.75 m, and 0.375 m. The figure clearly demonstrates the convergence of the RAO curves.

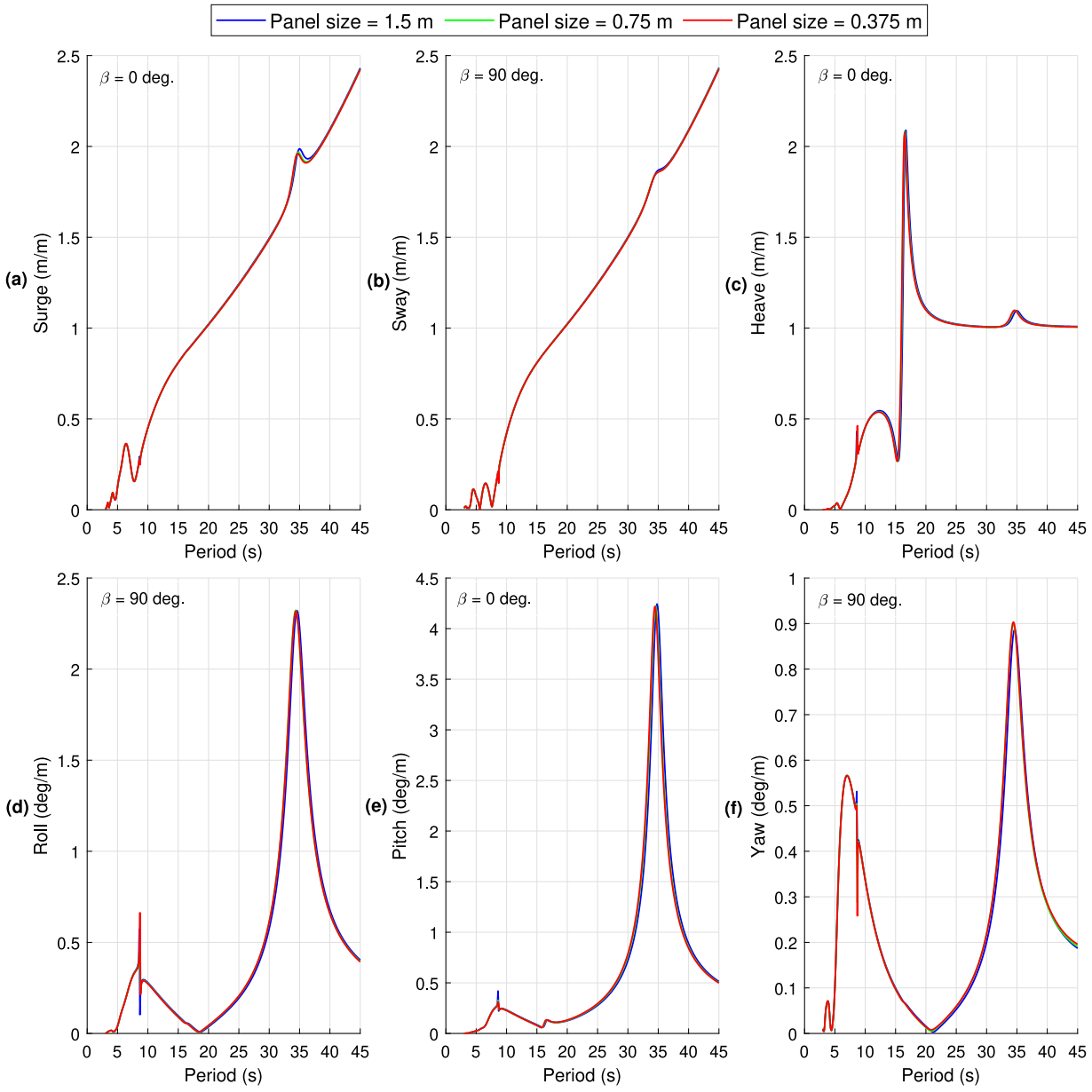

Fig. 20. Panel size sensitivity study using RAOs for FWT-OWCs system for (a) Surge. (b) Sway. (c) Heave. (d) Roll. (e) Pitch. (d) Yaw.

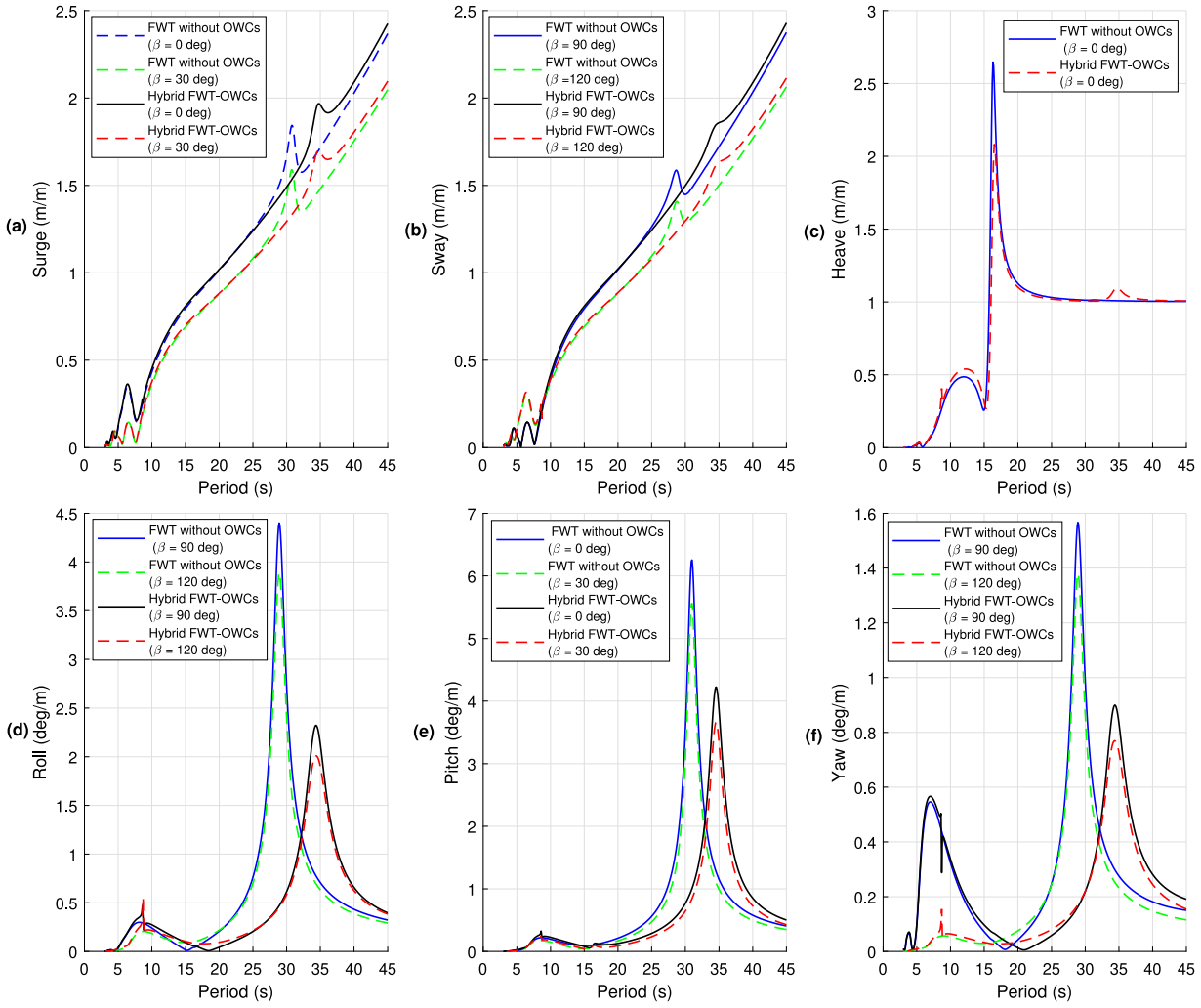

Fig. 21. RAOs for FWT without OWCs and hybrid FWT-OWCs systems for (a) Surge. (b) Sway. (c) Heave. (d) Roll. (e) Pitch. (d) Yaw.

Appendix B. Comparison study

For a more comprehensive understanding of the dynamic behavior of both the FWT without OWCs and the hybrid FWT-OWCs systems, a comparison of their Response Amplitude Operators (RAOs) for different states is presented in Fig. 21.

References

[1] F. Papi, A. Bianchini, Technical challenges in floating offshore wind turbine upscaling: A critical analysis based on the NREL 5 MW and IEA 15 MW reference turbines, Renew. Sustain. Energy Rev. 162 (2022) 112489.

[2] E. An, Strategy to Harness the Potential of Offshore Renewable Energy for a Climate Neutral Future, European Commission, Brussels, Belgium, 2020.

[3] K.A. Shah, Y. Li, R. Nagamune, Y. Zhou, W.U. Rehman, Platform motion minimization using model predictive control of a floating offshore wind turbine, Theor. Appl. Mech. Lett. 11 (5) (2021) 100295.

[4] H. Diken, S. Asiri, Vibration analysis of horizontal axis wind turbine considering tower-nacelle-foundation interaction, J. Vib. Eng. Technol. (2023).

[5] Z. Xu, J. Wei, S. Zhang, Z. Liu, X. Chen, Q. Yan, J. Guo, A state-of-the-art review of the vibration and noise of wind turbine drivetrains, Sustain. Energy Technol. Assess. 48 (2021) 101629.

[6] S. Fu, Y. Jin, Y. Zheng, L.P. Chamorro, Wake and power fluctuations of a model wind turbine subjected to pitch and roll oscillations, Appl. Energy 253 (2019) 113605.

[7] M.N. Haji, J.M. Kluger, T.P. Sapsis, A.H. Slocum, A symbiotic approach to the design of offshore wind turbines with other energy harvesting systems, Ocean Eng. 169 (2018) 673–681.

[8] H.M. Johlas, L.A. Martínez-Tossas, M.J. Churchfield, M.A. Lackner, D.P. Schmidt, Floating platform effects on power generation in spar and semisubmersible wind turbines, Wind Energy 24 (8) (2021) 901–916.

[9] A. Awada, R. Younes, A. Ilinca, Review of vibration control methods for wind turbines, Energies 14 (11) (2021) 3058.

[10] A. Saenz-Aguirre, E. Zulueta, U. Fernandez-Gamiz, A. Ulazia, D. Teso-Fz-Betono, Performance enhancement of the artificial neural network–based reinforcement learning for wind turbine yaw control, Wind Energy 23 (3) (2020) 676–690.

[11] S. Sarkar, B. Fitzgerald, B. Basu, Individual blade pitch control of floating offshore wind turbines for load mitigation and power regulation, IEEE Trans. Control Syst. Technol. 29 (1) (2020) 305–315.

[12] S. Sarkar, B. Fitzgerald, Vibration control of spar-type floating offshore wind turbine towers using a tuned mass-damper-inerter, Struct. Control Health Monit. 27 (1) (2020) e2471.

[13] Z. Zhao, K. Dai, E.R. Lalonde, J. Meng, B. Li, Z. Ding, G. Bitsuamlak, Studies on application of scissor-jack braced viscous damper system in wind turbines under seismic and wind loads, Eng. Struct. 196 (2019) 109294.

[14] C. Sun, V. Jahangiri, Bi-directional vibration control of offshore wind turbines using a 3D pendulum tuned mass damper, Mech. Syst. Signal Process. 105 (2018) 338–360.

[15] N. Navadeh, I. Goroshko, Y. Zhuk, F. Etminan Moghadam, A. Soleiman Fallah, Finite element analysis of wind turbine blade vibrations, Vibration 4 (2) (2021) 310–322.

[16] T.-t. Zhang, M. Elsakka, W. Huang, Z.-g. Wang, D.B. Ingham, L. Ma, M. Pourkashanian, Winglet design for vertical axis wind turbines based on a design of experiment and CFD approach, Energy Convers. Manage. 195 (2019) 712–726.

[17] Z. Zhao, R. Jiang, J. Feng, H. Liu, T. Wang, W. Shen, M. Chen, D. Wang, Y. Liu, Researches on vortex generators applied to wind turbines: A review, Ocean Eng. 253 (2022) 111266.

[18] K.A. Muhammed, C.R. Kannan, B. Stalin, Performance analysis of wind turbine blade materials using nanocomposites, Mater. Today: Proc. 33 (2020) 4353–4361.

[19] J. Cutler, M. Bashir, Y. Yang, J. Wang, S. Loughney, Preliminary development of a novel catamaran floating offshore wind turbine platform and assessment of dynamic behaviours for intermediate water depth application, Ocean Eng. 258 (2022) 111769.
[20] J.M. Hegseth, E.E. Bachynski, B.J. Leira, Effect of environmental modelling and inspection strategy on the optimal design of floating wind turbines, Reliab. Eng. Syst. Saf. 214 (2021) 107706.
[21] G. Ferri, E. Marino, Site-specific optimizations of a 10 MW floating offshore wind turbine for the Mediterranean sea, Renew. Energy 202 (2023) 921–941.
[22] J.M. Hegseth, E.E. Bachynski, A semi-analytical frequency domain model for efficient design evaluation of spar floating wind turbines, Mar. Struct. 64 (2019) 186–210.
[23] S. Zhou, K. Müller, C. Li, Y. Xiao, P.W. Cheng, Global sensitivity study on the semisubmersible substructure of a floating wind turbine: Manufacturing cost, structural properties and hydrodynamics, Ocean Eng. 221 (2021) 108585.
[24] G. Ferri, E. Marino, N. Bruschi, C. Borri, Platform and mooring system optimization of a 10 MW semisubmersible offshore wind turbine, Renew. Energy 182 (2022) 1152–1170.
[25] T. Wakui, A. Nagamura, R. Yokoyama, Stabilization of power output and platform motion of a floating offshore wind turbine-generator system using model predictive control based on previewed disturbances, Renew. Energy 173 (2021) 105–127.
[26] S. Quallen, T. Xing, CFD simulation of a floating offshore wind turbine system using a variable-speed generator-torque controller, Renew. Energy 97 (2016) 230–242.
[27] Z. Jiang, Z. Chen, W. Liu, Y. Liu, X. Wang, A review of individual pitch control for wind turbines, in: 2016 IEEE 11th Conference on Industrial Electronics and Applications (ICIEA), IEEE, 2016, pp. 399–404.
[28] P. Aboutalebi, F. M'zoughi, I. Garrido, A.J. Garrido, Performance analysis on the use of oscillating water column in barge-based floating offshore wind turbines, Mathematics 9 (5) (2021) 475.
[29] J. Hu, B. Zhou, C. Vogel, P. Liu, R. Willden, K. Sun, J. Zang, J. Geng, P. Jin, L. Cui, et al., Optimal design and performance analysis of a hybrid system combing a floating wind platform and wave energy converters, Appl. Energy 269 (2020) 114998.
[30] J. Sarmiento, A. Iturrioz, V. Ayllón, R. Guanche, I. Losada, Experimental modelling of a multi-use floating platform for wave and wind energy harvesting, Ocean Eng. 173 (2019) 761–773.
[31] C. Michailides, Z. Gao, T. Moan, Experimental and numerical study of the response of the offshore combined wind/wave energy concept SFC in extreme environmental conditions, Mar. Struct. 50 (2016) 35–54.
[32] E.E. Bachynski, T. Moan, Point absorber design for a combined wind and wave energy converter on a tension-leg support structure, in: International Conference on Offshore Mechanics and Arctic Engineering, Vol. 55423, American Society of Mechanical Engineers, 2013, V008T09A025.
[33] N. Ren, Z. Ma, B. Shan, D. Ning, J. Ou, Experimental and numerical study of dynamic responses of a new combined TLP type floating wind turbine and a wave energy converter under operational conditions, Renew. Energy 151 (2020) 966–974.
[34] A. Aubault, M. Alves, A.n. Sarmento, D. Roddier, A. Peiffer, Modeling of an oscillating water column on the floating foundation WindFloat, in: International Conference on Offshore Mechanics and Arctic Engineering, Vol. 44373, 2011, pp. 235–246.
[35] P. Aboutalebi, F. M'zoughi, I. Martija, I. Garrido, A.J. Garrido, Switching control strategy for oscillating water columns based on response amplitude operators for floating offshore wind turbines stabilization, Appl. Sci. 11 (11) (2021) 5249.
[36] P. Aboutalebi, F. M'zoughi, I. Garrido, A.J. Garrido, A control technique for hybrid floating offshore wind turbines using oscillating water columns for generated power fluctuation reduction, J. Comput. Des. Eng. 10 (1) (2023) 250–265.
[37] D. Zhang, Z. Chen, X. Liu, J. Sun, H. Yu, W. Zeng, Y. Ying, Y. Sun, L. Cui, S. Yang, et al., A coupled numerical framework for hybrid floating offshore wind turbine and oscillating water column wave energy converters, Energy Convers. Manage. 267 (2022) 115933.
[38] G. DNV, Sesam User Manual-Genie, DNV GL Software, 2016.
[39] G. DNV, Sesam User Manual-Hydrod, DNV GL, Høvik, Norway, 2013.
[40] G. DNV, Sesam User Manual-Wadam, DNV GL Software, 2017.
[41] C.E. Silva de Souza, P.A. Berthelsen, L. Eliassen, E.E. Bachynski, E. Engebretsen, H. Haslum, Definition of the INO WINDMOOR 12 MW base case floating wind turbine, 2021.
[42] F. Shiravani, J.A. Cortajarena, P. Alkorta, O. Barambones, A nonlinear generalized predictive control scheme for the oscillating water column plants, Ocean Eng. 284 (2023) 115150.
[43] A.J. Garrido, I. Garrido, M. Amundarain, M. Alberdi, M. De la Sen, Sliding-mode control of wave power generation plants, IEEE Trans. Ind. Appl. 48 (6) (2012) 2372–2381.
[44] D.N. Veritas, Recommended Practice: Environmental Conditions and Environmental Loads, DNV-GL, Oslo, Norway, 2010.
[45] Norwegian maritime authority, regulations of 20 december 1991 no. 878 on stability, watertight subdivision and watertight/weathertight means of closure on mobile offshore units, 1991, https://www.sdir.no/en/shipping/legislation/regulations/stability-watertight-subdivision-and-watertight-weathertight-closing-means-on-mobile-offshore-units/.
[46] T. Fossen, Handbook of Marine Craft Hydrodynamics and Motion Control, Wiley, 2021.